

# Modeling of Electron Mobility Degradation for HfSiON MISFETs

Hiroyoshi Tanimoto\*, Masaki Kondo\*, Toshiyuki Enda\*, Nobutoshi Aoki\*, Ryosuke Iijima†, Takeshi Watanabe\*, Mariko Takayanagi\* and Hidemi Ishiuchi\*

\* Center for Semiconductor Research & Development, Toshiba Corp. Semiconductor Company  
8, Shinsugita-cho, Isogo-ku, Yokohama 235-8522, Japan

TEL: +81-45-770-3645, FAX: +81-45-770-3571, E-Mail: hiroyoshi.tanimoto@toshiba.co.jp

† Advanced LSI Technology Laboratory, Corporate Research & Development Center, Toshiba Corp.

## I. INTRODUCTION

High- $\kappa$  insulators are to be utilized as gate dielectric films for advanced CMOS devices. One of main problems of the high- $\kappa$  MISFETs is reduced carrier mobility compared with that of thermally grown pure SiO<sub>2</sub> MOSFETs [1]–[3], since lower carrier mobility degrades the device performance. We investigate the electron mobility degradation for HfSiON MISFETs and find that there are two sources of the mobility degradation; one is Coulomb scattering caused by fixed charges in HfSiON films and the other is phonon scattering by interfacial thin oxynitrided (SiON) layer; and HfSiO-related remote phonon scattering is not dominant. The mobility degradation caused by the Coulomb scattering and SiON phonon scattering is separated into two components and we develop an empirical mobility model for HfSiON devices that enables accurate simulation of electrical characteristics of the HfSiON devices.

## II. MOBILITY DEGRADATION OF HfSiON DEVICES COMPARED WITH SiO<sub>2</sub> DEVICES

Effective electron mobility for HfSiON n-MISFETs and for control thermal SiO<sub>2</sub> MOSFETs is measured by the conventional split  $C-V$  method. The results for substrate acceptor concentration  $N_A = 3 \times 10^{16} \text{ cm}^{-3}$  are shown in Fig. 1 [4]. As shown in this figure, the effective mobility for HfSiON MISFETs is reduced compared with that for the control SiO<sub>2</sub> MOSFETs.

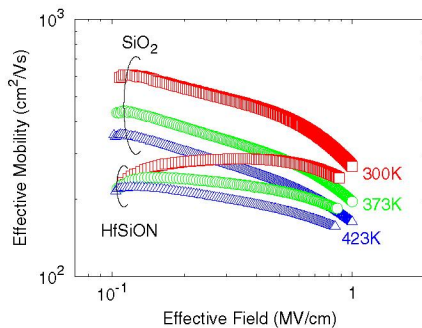


Fig. 1. Measured effective electron mobility for HfSiON MISFETs and pure SiO<sub>2</sub> MOSFETs as a function of effective field at 300–423K. Substrate concentration  $N_A$  is  $3 \times 10^{16} \text{ cm}^{-3}$ .

The mobility reduction for the HfSiON devices can be extracted using Matthiessen's rule:

$$1/\mu_{\text{HfSiON}} = 1/\mu_{\text{SiO}_2} + 1/\Delta\mu, \quad (1)$$

where  $\mu_{\text{HfSiON}}$  is the effective mobility for HfSiON devices,  $\mu_{\text{SiO}_2}$  is the effective mobility for SiO<sub>2</sub> devices and  $\Delta\mu$  is the mobility reduction caused by the HfSiON gate insulators compared with the SiO<sub>2</sub> films. The extracted mobility reduction  $\Delta\mu$  is plotted in Fig. 2 as a function of inversion electron density  $N_s$ . As can be seen in this figure, the mobility degradation  $\Delta\mu$  is proportional to the power of  $N_s$ ;  $\Delta\mu \propto N_s^\alpha$ ; and the slope  $\alpha$  strongly depends on the temperature and the substrate acceptor concentration.

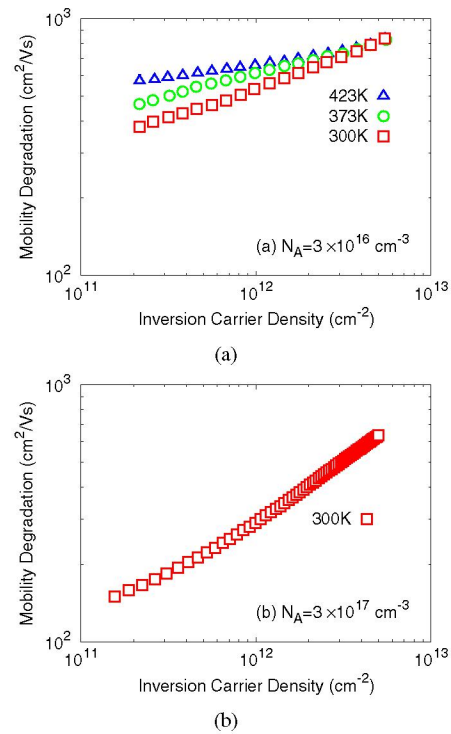


Fig. 2. Extracted mobility degradation of HfSiON MISFETs compared with pure SiO<sub>2</sub> MOSFETs. (a)  $N_A = 3 \times 10^{16} \text{ cm}^{-3}$  and (b)  $3 \times 10^{17} \text{ cm}^{-3}$ .

In order to explain the dependence of the mobility degrada-

tion  $\Delta\mu$  on the electron sheet density  $N_s$  and the temperature  $T$ , we firstly investigated the remote Coulomb scattering (RCS) and the remote phonon scattering (RPS).

In Figs. 3(a) and (b), RCS-limited mobility  $\mu_C$  and RPS-limited mobility  $\mu_P$  are schematically illustrated as a function of  $N_s$  and  $T$ . As shown in these figures, the limited mobility for these scattering mechanisms is proportional to the power of  $N_s$ ;  $\mu_C \propto N_s^{\alpha_C}$  and  $\mu_P \propto N_s^{\alpha_P}$ ; and the slopes for RCS- and RPS-limited mobility;  $\alpha_C$  and  $\alpha_P$ ; weakly depend on  $T$ . The slopes  $\alpha_C$  and  $\alpha_P$  are quite different. The RCS-limited mobility becomes higher at strong inversion condition and at higher temperature, since screening effect becomes larger at higher carrier density and at higher temperature. On the other hand, the RPS-limited mobility becomes lower at strong inversion condition and higher temperature, since phonon-electron interaction becomes stronger under higher electric field and at higher temperature.

By comparing Fig. 2 with Figs. 3(a) and (b), it is clear that the temperature dependence of the slope measured for HfSiON devices can be qualitatively explained by neither RCS nor RPS. Furthermore, a combination of the both RCS and RPS mechanisms leads to a complicated  $N_s$  dependence of the limited mobility  $\mu_{CP}$  as shown in Fig. 4. Though the temperature dependence of the slope can be partially explained,  $\mu_{CP}$  is not proportional to  $N_s^\alpha$  as shown in Fig. 2.

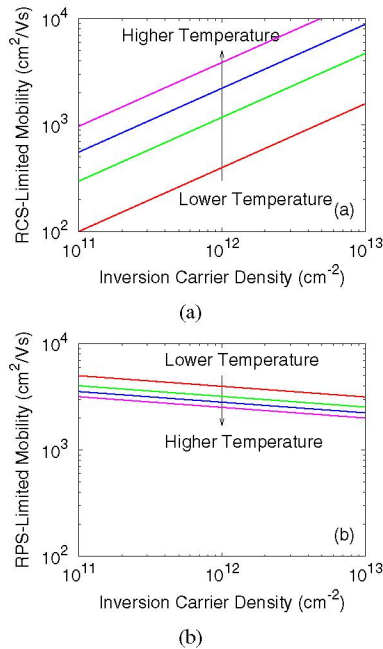


Fig. 3. Schematic drawings of (a) RCS-limited mobility  $\mu_C$  and (b) RPS-limited mobility  $\mu_P$  as a function of inversion carrier density and temperature. Both RCS and RPS limited mobility is proportional to the power of electron density  $N_s^\alpha$ . The slope  $\alpha$  weakly depends on temperature but differs greatly between RCS and RPS.

### III. MOBILITY DEGRADATION OF HFSiON DEVICES COMPARED WITH SiON DEVICES

As described in the previous section, the mobility degradation for the HfSiON devices compared with the pure SiO<sub>2</sub>

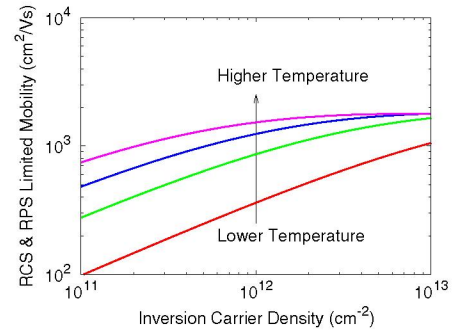


Fig. 4. Schematic limited mobility caused by RCS and RPS  $\mu_{CP}$  as a function of inversion carrier density and temperature. These two scattering mechanisms are combined by using the well-known Matthiessen's rule.

devices was not ascribable to simple RCS and RPS mechanisms. Changing our viewpoint, we focused on nitrogen atoms in interfacial thin SiO<sub>2</sub> between Si substrate and HfSiON dielectric. The N atoms were introduced by Ar/N<sub>2</sub> plasma nitridation process following HfSiO deposition to suppress the phase separation of HfSiO [4], [5]. Since we thought most N atoms were making bonds with Hf atoms in HfSiON and the interfacial oxide had the same characteristics as the usual thermal oxide, the effective mobility of HfSiON devices was compared with that of the control thermal SiO<sub>2</sub> devices. Koike *et al.* showed that N atoms were creating not only Hf-N bonds but also Si-N bonds and the Si-N bonds were increased with increasing N atoms in HfSiON while Si-O bonds were decreased [6]. This indicates that the interfacial SiO<sub>2</sub> between HfSiON and Si substrate is likely nitrided and will have similar characteristics to SiON as shown in Fig. 5 and the mobility degradation of HfSiON devices should be discussed in comparison with the mobility for the SiON devices.

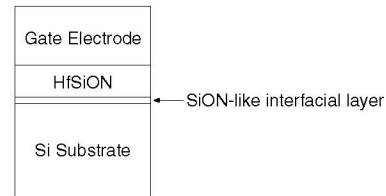


Fig. 5. Schematic cross-section of HfSiON gate stack. Interfacial oxide between HfSiON and Si substrate is nitrided and has similar characteristics to SiON.

In Fig. 6, backside SIMS (Secondary Ion Mass Spectroscopy) results are plotted. As shown in this figure, there are huge numbers of oxygen atoms at the bottom of HfSiON films (the left side of the figure) and this indicates existence of interfacial oxide layer between HfSiON and Si substrate. Also it is shown that the concentration of nitrogen atoms is high at interfacial layer. Bonding state of the interfacial layer is not clear, but it is possible that the interfacial layer has characteristics similar to those of SiON.

It is well known that the electron mobility of SiON MIS-FETs is lower at moderate electric field but higher at high electric field compared with that for SiO<sub>2</sub> MOSFETs [7].

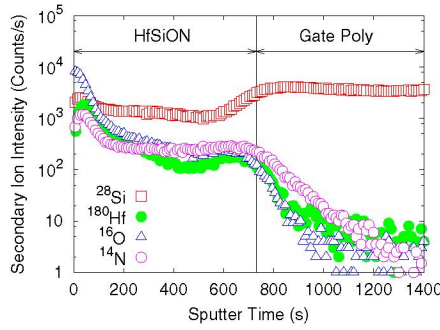


Fig. 6. Backside SIMS results are plotted as a function of the position from the Si substrate. The left side of the figure corresponds to the top of the substrate. This figure shows existence of interfacial oxide between HfSiON and Si substrate and N atoms exist at the interfacial region.

An empirical model of effective mobility for SiON MISFETs  $\mu_{SiON}$  in  $\text{cm}^2/\text{Vs}$  is shown in Eq. (2) [8] and is plotted in Fig. 7.

$$\mu_{SiON} = \left[ \frac{T_0^{2.1}}{1400} + 2.4 \times 10^{-3} T_0^{1.82} E_{eff}^{0.33} + 6.5 \times 10^{-4} E_{eff}^2 \right]^{-1}, \quad (2)$$

where  $E_{eff}$  is the effective field in  $\text{MV}/\text{cm}$  and  $T_0 = T/300$ . The second and the third terms of RHS of Eq. (2) express phonon and surface roughness scattering mechanisms, respectively [9]. The following model is used as bulk Coulomb scattering limited mobility  $\mu_C$  [8];

$$\mu_C = \frac{4.3 \times 10^{11}}{N_A^{1.15}} N_s, \quad (3)$$

where  $N_A$  is substrate acceptor concentration in  $\text{cm}^{-3}$  and  $N_s$  is inversion electron density in  $\text{cm}^{-2}$ . By using Fig. 1 and Eqs. (2) and (3), the mobility degradation  $\Delta\mu'$  of HfSiON devices compared with the SiON devices is extracted:

$$1/\mu_{HfSiON} = 1/\mu_{SiON} + 1/\mu_C + 1/\Delta\mu'. \quad (4)$$

The extracted mobility degradation  $\Delta\mu'$  is plotted in Figs. 8(a) and (b) for devices with  $N_A = 3 \times 10^{16} \text{cm}^{-3}$  and  $3 \times 10^{17} \text{cm}^{-3}$ , respectively. As shown in these figures, the mobility degradation  $\Delta\mu'$  is proportional to the power of  $N_s$  and the slope is almost independent of temperature  $T$ . This is Coulombic scattering behavior as schematically shown in Fig. 3(a).

This degradation is caused by the RCS of HfSiON's fixed charges. In the weak inversion condition, the degradation for higher substrate acceptor density is worse than that for lower substrate acceptor density. It is because electron occupation rate of the lowest subband is higher for higher substrate acceptor density. Electrons in the lowest subband are closer to HfSiON's fixed charges than these in the upper subbands and the scattering rate becomes higher. So the RCS-limited mobility becomes lower for higher substrate acceptor density.

The extracted mobility degradation can be expressed by the following equation and is plotted by solid lines in Fig. 8.

$$\Delta\mu' = 240 \left( \frac{N_A}{3 \times 10^{16}} \right)^{-0.30} T_0^{2.1} \left( \frac{N_s}{10^{11}} \right)^{0.40+0.035 \log \left( \frac{N_A}{3 \times 10^{16}} \right)}. \quad (5)$$

The developed mobility degradation model for HfSiON devices is implemented into in-house device simulator DSStation.  $C_{gc} - V_g$  and  $I_d - V_g$  characteristics of HfSiON MISFETs are simulated with the developed mobility model and are shown in Figs. 9 and 10. For comparison, simulated results with the conventional SiON mobility model [8] are shown in Fig. 11. As shown in these figures, the developed mobility model has good accuracy and enables accurate simulation of HfSiON MISFETs' characteristics.

The mobility degradation for SiON MISFETs is discussed in comparison with  $\text{SiO}_2$  MOSFETs. In Fig. 12, the effective mobility for pure  $\text{SiO}_2$  MOSFETs and SiON MISFETs is plotted as a function of effective field. The mobility degradation for SiON MISFETs compared with  $\text{SiO}_2$  MOSFETs is extracted and plotted in Fig. 13. As shown in these figures, at moderate electric field, the degradation for SiON MISFETs is higher at higher temperature and shows dependence similar to that of phonon scattering. On the other hand, at high electric field, suppression of surface roughness scattering is observed which is typical for SiON n-type MISFETs [7].

#### IV. CONCLUSION

The electron mobility degradation for HfSiON MISFETs was investigated. We found that the degradation had two origins: interfacial thin SiON and HfSiON's fixed charges. HfSiO-related phonon scattering is not observed but SiON phonon scattering is observed. The degradation caused by the fixed charges was extracted from experimental data using an SiON mobility model and a simple form of the degradation was presented.

#### ACKNOWLEDGMENTS

We are grateful to T. Ishihara, Y. Nakasaki, M. Nakamura and Y. Toyoshima for fruitful discussion and encouragement.

#### REFERENCES

- [1] M. V. Fischetti, D. A. Neumayer and E. A. Cartier, J. Applied Phys., **90**, p. 4587 (2001).
- [2] S. Saito, D. Hisamoto, S. Kimura and M. Hiratani, IEDM Tech. Dig., p. 797 (2003).
- [3] K. Torii, Y. Shimamoto, S. Saito, K. Obata, T. Yamauchi, D. Hisamoto, T. Onai and M. Hiratani, Microelectron. Eng. **59**, p. 447 (2003).
- [4] R. Iijima, M. Takayanagi, T. Ishihara, T. Yamaguchi and A. Nishiyama, Ext. Abs. SSDM 2004, p. 32 (2004).
- [5] K. Sekine, S. Inumiya, M. Sato, A. Kaneko, K. Eguchi and Y. Tsunashima, IEDM Tech. Dig., p. 103 (2003).
- [6] M. Koike, T. Ino, Y. Kamimuta, M. Koyama, Y. Kamata, M. Suzuki, Y. Mitani, A. Nishiyama and Y. Tsunashima, IEDM Tech. Dig., p. 107 (2003).
- [7] M. Takayanagi-Takagi and Y. Toyoshima, IEDM Tech. Dig., p. 575 (1998).
- [8] M. Kondo and H. Tanimoto, IEEE Trans. Electron Devices, **48**, p. 265 (2001).
- [9] S. Takagi, M. Iwase and A. Toriumi, IEDM Tech. Dig., p. 398 (1988).

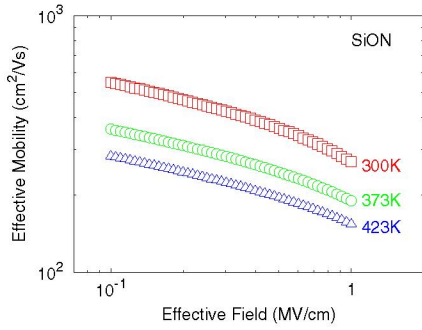


Fig. 7. An effective mobility model for SiON MISFETs expressed by Eq. (2). This model is used to extract mobility degradation  $\Delta\mu'$  of HfSiON MISFETs compared with SiON MISFETs.

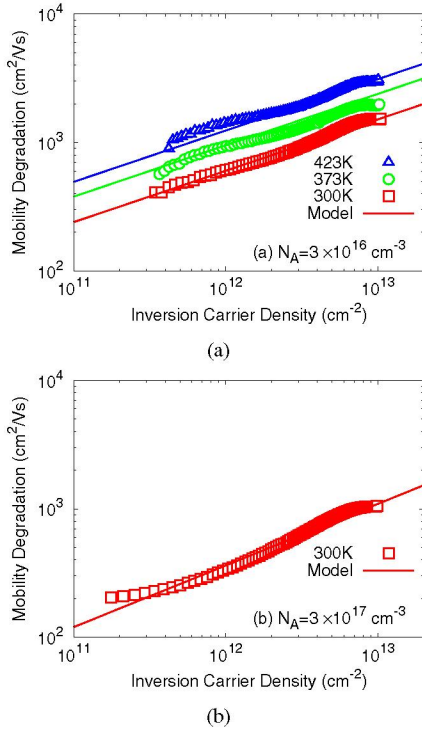


Fig. 8. Extracted mobility degradation  $\Delta\mu'$  of HfSiON MISFETs compared with SiON MISFETs as a function of inversion electron density. The substrate acceptor concentration is (a)  $N_A = 3 \times 10^{16} \text{ cm}^{-3}$  and (b)  $3 \times 10^{17} \text{ cm}^{-3}$ . The extraction is performed using measured HfSiON effective mobility and SiON mobility model expressed by Eq. (2). Solid lines are modeled mobility degradation expressed by Eq. (5).

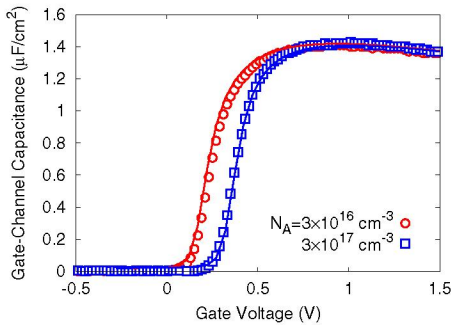


Fig. 9. Measured (symbols) and simulated (lines)  $C_{gc} - V_g$  characteristics of HfSiON MISFETs.  $L_g = 10 \mu\text{m}$  and  $W = 100 \mu\text{m}$ .  $T = 300\text{K}$ .  $N_A = 3 \times 10^{16} \text{ cm}^{-3}$  and  $3 \times 10^{17} \text{ cm}^{-3}$ .

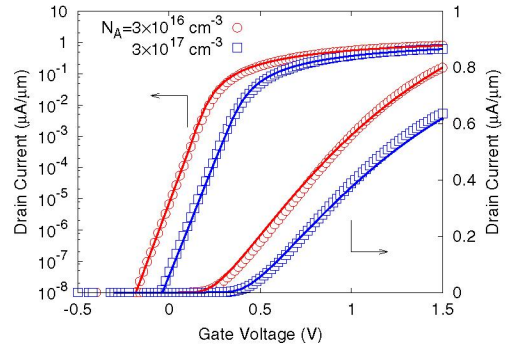


Fig. 10. Measured (symbols) and simulated (lines)  $I_d - V_g$  characteristics of HfSiON MISFETs. Simulation is performed with the developed mobility model.  $L_g = 10 \mu\text{m}$  and  $W = 100 \mu\text{m}$ .  $T = 300\text{K}$ .  $N_A = 3 \times 10^{16} \text{ cm}^{-3}$  and  $3 \times 10^{17} \text{ cm}^{-3}$ .

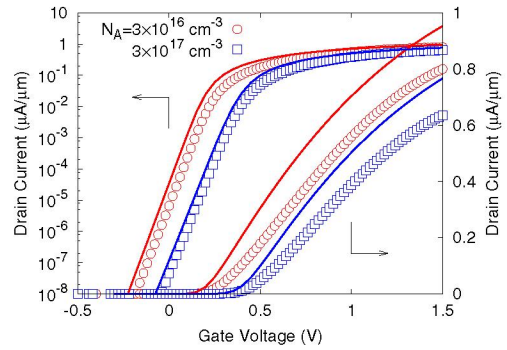


Fig. 11. Simulated  $I_d - V_g$  characteristics with the conventional SiON mobility model are shown for comparison. The conventional mobility model has poor accuracy to simulate HfSiON MISFETs' characteristics.

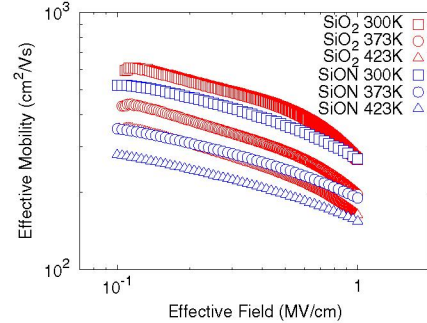


Fig. 12. Effective mobility for SiO₂ MOSFETs and SiON MISFETs is plotted as a function of effective field. Substrate acceptor concentration  $N_A$  is  $3 \times 10^{16} \text{ cm}^{-3}$ .

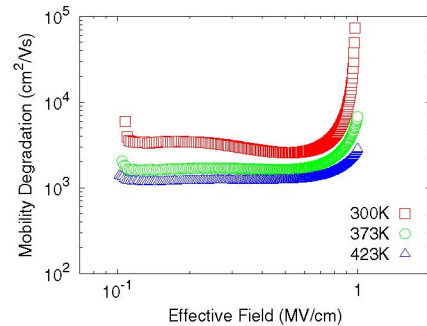


Fig. 13. Effective mobility degradation for SiON MISFETs compared with SiO₂ MOSFETs is plotted as a function of effective field.